

Synthesis, characterization, crystal structure and theoretical approach of (*E*)-2-[(3-carboxylphenylimino)methylene]phenoxyacetic acid

Shi-Liang Chen ^{a,b}, Zheng Liu ^{a,*}, Guo-Cheng Han ^{c,*}

^a College of Chemical and Biological Engineering, Guilin University of Technology, Guilin 541004, PR China

^b Shaanxi Xianyang Chemical Industrial Co. Ltd., Xianyang 712000, PR China

^c School of Life and Environmental Sciences, Guilin University of Electronic Technology, Guilin 541004, PR China

HIGHLIGHTS

- ▶ Aromatic carboxylic acid compound had been synthesized and characterized.
- ▶ Part of crystal structure of compound shown formation of centrosymmetric $R_2^2(8)$ dimer.
- ▶ Compound engendered strong fluorescence emission in purple region.
- ▶ Redox action of compound is very difficult.
- ▶ DFT calculation results are good agreed with experimental data.

ARTICLE INFO

Article history:

Received 22 April 2012

Received in revised form 8 October 2012

Accepted 9 October 2012

Available online 17 October 2012

Keywords:

Schiff bases

Crystal structure

Fluorescence property

Electrochemical property

Vibrational assignment

DFT calculations

ABSTRACT

The title compound, (*E*)-2-[(3-carboxylphenylimino)methyl]phenoxyacetic acid ($C_{16}H_{13}NO_5$), had been synthesized and characterized by FT-IR, UV-vis spectrum, fluorescence spectrum, elemental analysis, electrochemistry and single crystal X-ray diffraction techniques. Crystallographic analysis show that non-covalent C—H...O and inter-molecular hydrogen bonding interactions assemble the 3D network structure of the title compound. Moreover, the vibrational frequencies of the title compound in the ground state had been calculated using the Hartree-Fock (HF) and density functional methods (B3LYP) with 6-31G* and 6-31+G(d) basis set, respectively. The results of the calculational optimized molecular structure, absorption spectra and fluorescence emission are exhibited and compared with the experimental results of X-ray diffraction, UV-vis spectrum and fluorescence spectrum, respectively. In addition, frontier molecular orbitals (FMOs), mulliken charges, wiberg bond index and molecular electrostatic potential (MEP) were executed by the RB3LYP/6-31+G(d) method.

© 2012 Elsevier B.V. All rights reserved.

1. Introduction

Schiff bases and aromatic carboxyl derivatives had been extensively investigated in the past decades, because they own properties of strong metals chelating tendency, plant growth regulating activity, photochemistry and their vital role in photopolymerization activity [1–7]. Many of these compounds possess biochemical and pharmacological properties, especially their antimicrobial, anti-tumor and anti-inflammatory activity, which may afford them potential as therapeutic agents and make them very useful [8,9]. In addition, they are widely used as ligands in the field of coordination chemistry as well as in diverse fields of

chemistry and biochemistry [10,11]. Numerous reports on metal-organic frameworks based on Schiff base ligands have been reported [12,13]. In recent years, density functional theory (DFT) has been a shooting star in theoretical modelling. The development of better and better exchange-correlation functional made it possible to calculate many molecular properties with comparable accuracies to traditional correlated abinitio methods [14].

In this study, the crystal structure of (*E*)-2-[(3-carboxylphenylimino)methyl]phenoxyacetic acid was determined by single crystal X-ray diffraction technique and characterized by FT-IR, fluorescence spectrum and UV-vis spectrum. In order to get more insight on stability and its activity areas, the computational studies at DFT and HF levels were carried out. The excitation energies were obtained using DFT calculations starting from optimized geometry. We hope our work will be helpful for the further studies on their potential applications.

* Corresponding authors. Tel.: +86 773 5896453 (Z. Liu), tel.: +86 773 2291002 (G.-C. Han).

E-mail addresses: lisa4.6@163.com (Z. Liu), hangc81@guet.edu.cn (G.-C. Han).

2. Experimental

2.1. Materials and physical measurements

The reagents were commercially available and were used without further purification for the synthesis. Carbon, Hydrogen and Nitrogen were estimated micro-analytically by Vario ELIII elemental instrument. FT-IR spectrum of the title compound was recorded on a Shimadzu FTIR-8400 spectrometer in KBr disk. Elemental analyses for carbon, hydrogen and nitrogen were performed by a Vario ELI elemental instrument. The FT-IR spectra were recorded in the range of 4000–400 cm^{-1} using KBr pellets on a Shimadzu FT-IR-8400 spectrophotometer. UV–vis spectra were recorded in N,N-dimethylformamide solution using GBC UV–vis spectrophotometer. The emission/excitation spectra were measured on a Hitachi RF-5301 fluorescence spectrophotometer. The electron transfer behavior of the complex was examined using cyclic voltammogram on a CHI-860D electrochemical analysis system by a three-electrode cell at room temperature. A glass carbon (GC) working (3 mm in diameter), a saturated calomel electrode (SCE) as reference electrode and a platinum wire electrode as auxiliary electrode.

2.2. Preparation of the title compound

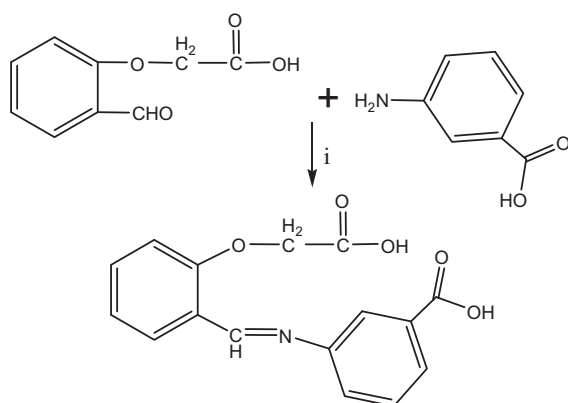
2.2.1. Synthesis of the *o*-formylphenoxyacetic acid

The *o*-formylphenoxyacetic acid had been obtained by reaction of salicylaldehyde and chloroacetic acid according to the literature preparation [15], m.p.: 131–133 °C, which is accordant for literature values.

2.2.2. Synthesis of the title compound

A solution of *o*-formylphenoxyacetic acid (0.90 g, 5 mmol) in methanol (20 mL) was added dropwise with stirring at room temperature to a solution of 3-formylbenzoic acid (0.69 g, 5 mmol) in methanol (15 mL). The mixture was refluxed with stirred for 3 h at 70 °C until yellowish precipitate was formed. The precipitate was collected by filtration and washed with ethanol (Scheme 1). At the same time, the production was desiccated in the loft drier (yield: 30%, m.p.: 220–222 °C). The single crystal of the complex, suitable for X-ray diffraction study was cultured from the filtered reaction solution by a slow evaporation method at room temperature for 2 weeks.

Anal. Calcd. for $\text{C}_{16}\text{H}_{13}\text{NO}_5$: C 64.21, H 4.38, N 4.68%. Found: C 64.25, H 4.41, N 4.63%.



Scheme 1. The reaction process of the title compound **1**. (i): CH_3OH reflux 3 h.

Table 1

Crystal data and structure refinement for **1**.

CCDC reference no.	821265
Empirical formula	$\text{C}_{16}\text{H}_{13}\text{NO}_5$
Formula weight	299.27
Temperature (K)	293(2)
Wavelength (Å)	0.71073
Crystal system	Triclinic
Space group	$P-1$
Unit cell dimensions (Å, °)	$a = 8.0822(8)$, $b = 9.4699(11)$, $c = 0.3581(15)$ $\alpha = 67.1770(10)$, $\beta = 82.465(2)$, $\gamma = 5.8130(10)$
Volume (Å ³)	707.85(15)
Z	2
Density (calculated) (Mg/m ³)	1.404
Absorption coefficient (mm ⁻¹)	0.106
$F(000)$	312
Crystal form, color	Block, yellow
Crystal size (mm)	$0.31 \times 0.28 \times 0.14$
θ range for data collection (°)	2.39–25.02
Index ranges	$-9 \leq h \leq 8$, $-10 \leq k \leq 11$, $-12 \leq l \leq 12$
Reflections collected	3731
Independent reflections (R_{int})	2461 (0.0368)
Refinement method	Full-matrix least-squares on F^2
Data/restraints/parameters	2461/2/201
Goodness-of-fit on F^2	1.203
Final R indices [$I > 2\sigma(I)$]	$R_1 = 0.0814$, $wR_2 = 0.1918$
R indices (all data)	$R_1 = 0.1262$, $wR_2 = 0.2103$
Weighting scheme	Calc. $w = 1/[\sigma^2(F_o^2) + (0.0479P)^2 + 1.1781P]$ where $P = (F_o^2 + 2F_c^2)/3$
Largest diff. peak and hole (e Å ⁻³)	0.254 and -0.238

2.3. X-ray crystal structure determination

A good block single crystal suitable with dimensions $0.31 \times 0.28 \times 0.14$ mm was mounted on goniometer and data collection was performed on a CCD area detector diffractometer by the φ and ω scan technique using graphite-monochromatic Mo K α radiation ($\lambda = 0.71073$ Å) at 293(2) K. In the range of $2.39^\circ \leq \theta \leq 25.02^\circ$, reflections were 3731 collected including 2461 unique ones ($R_{\text{int}} = 0.0368$), of which were observed with $I > 2\sigma(I)$ (1533 observed reflections). The structures were solved by direct methods with SHELXS-97 [16], and non-hydrogen atoms were refined anisotropically by full-matrix least-squares on F^2 using the SHELXTL-97 [17] program. H atoms on O atoms were located in a difference Fourier map and refined freely. H atoms attached to C atoms were refined as riding on their parent C atoms. Crystal data and refinement parameters are listed in Table 1 and selected bond length, angles and torsion angles are reported in Table 2.

2.4. Computational methods

The starting atomic coordinates were taken from the final X-ray refinement cycle. The geometry optimizations were performed at the RB3LYP/6-31+G(d) and RHF/6-31G* levels with the Gaussian 03 W program package [18,19]. The vibrational analysis has been performed to convince that all normal mode frequencies are real and non-negative and the calculated structures are stable. The Mulliken charge analysis, Frontier molecular orbitals (FMOs), molecular electrostatic potential (MEP) [20] were performed at the RB3LYP/6-31+G(d) levels, respectively. For the calculations of the Wiberg bond index, the same levels of theory RB3LYP/

Table 2

The experimental and optimized bond lengths (Å), angles (°) and torsion angles (°) for compound.

Bond lengths	Experimental	Calculated	
		RB3LYP/6-31+G(d)	RHF/6-31G*
N(1)—C(8)	1.289(6)	1.2843	1.2577
N(1)—C(4)	1.426(6)	1.4063	1.407
O(1)—C(1)	1.246(5)	1.2173	1.1907
O(2)—C(1)	1.287(5)	1.3602	1.3303
O(3)—C(10)	1.374(5)	1.3700	1.3523
O(3)—C(16)	1.421(5)	1.4066	1.385
O(4)—C(15)	1.328(5)	1.357	1.3299
O(5)—C(15)	1.186(5)	1.2055	1.181
C(1)—C(2)	1.488(7)	1.4868	1.4876
C(2)—C(3)	1.391(6)	1.4018	1.3903
Bond angles			
C(8)—N(1)—C(4)	117.8(4)	119.7769	119.9002
C(10)—O(3)—C(16)	117.2(3)	119.1282	120.6502
O(1)—C(1)—O(2)	122.7(5)	121.6108	121.7831
C(7)—C(2)—C(3)	120.1(5)	120.3467	120.5085
C(3)—C(4)—N(1)	122.4(4)	123.1786	123.346
C(5)—C(4)—N(1)	118.5(4)	117.7953	117.6059
N(1)—C(8)—C(9)	124.3(4)	121.6591	121.4163
O(3)—C(10)—C(11)	123.7(4)	123.6839	123.6189
O(3)—C(10)—C(9)	116.2(4)	115.8212	115.9049
O(5)—C(15)—O(4)	125.8(5)	123.8978	123.8079
O(5)—C(15)—C(16)	126.3(4)	126.872	126.6267
O(4)—C(15)—C(16)	107.9(4)	109.2301	109.5652
O(3)—C(16)—C(15)	109.4(4)	108.2571	108.199
Torsion angles			
O(1)—C(1)—C(2)—C(7)	−2.3(7)	−2.096	1.8127
O(2)—C(1)—C(2)—C(7)	177.5(5)	177.9291	178.1643
C(2)—C(3)—C(4)—N(1)	−178.7(4)	−178.3811	−178.9631
C(8)—N(1)—C(4)—C(3)	−43.3(7)	−40.3866	41.9592
C(8)—N(1)—C(4)—C(5)	139.6(5)	142.7538	140.706
C(4)—N(1)—C(8)—C(9)	177.3(4)	176.8407	178.66
C(10)—O(3)—C(16)—C(15)	168.6(4)	179.8806	179.7091
O(4)—C(15)—C(16)—O(3)	176.2(4)	179.4352	179.3484

6-31+G(d) and RHF/6-31G*, were used. The experimental and theoretical results are presented in Tables 2 and 4. No constraints to bonds, angles or dihedral angles were applied in the calculations and all atoms were free to optimize.

3. Results and discussion

3.1. Crystal structure

The X-ray structural determination at 293(2) K of the title compound, confirms the assignment of its structure from spectroscopic data. The molecular structure of the title compound is shown in Fig. 1, in which displacement ellipsoids are drawn at the 30% probability level and the formation of centrosymmetric R dimer of the title compound is shown in Fig. 2, the perspective view of the crystal packing is shown in Fig. S1. Selected bonds lengths, angles and torsion angles are listed in Table 2. Table 3 presents bond lengths and angles of the hydrogen bonds. All of the bond lengths and bond angles in phenyl rings are in the normal range. The distances (C—X, X = O, C, N) are closer than these the reported works [21–24]. Although in one molecule, the two phenyl rings are not coplanar with the dihedral angle of 29.5°, which are imposed from the intra-molecular biggish repulsion. In the crystal lattice, there are two potentially intermolecular interactions (O—H···Y, Y = O, N), details of which are given in Table 3 and Fig. 2. The intermolecular complementary O2—H2···O1 hydrogen bonds form centrosymmetric dimmers, and generating $R_2^2(8)$ supra-molecular synthon [25] (Fig. 2). O2A atom in the molecule at (x, y, z) and O2B atom in the molecule at (2 − x, 1 − y, 2 − z) act as donors to O1B atom in the molecule at (2 − x, 1 − y, 2 − z) and O1A atoms in the molecule at (x, y, z), respectively. The distance of C···O is changed from 3.18 to 3.42 Å and the C—H···O angle is changed from 118° to 144° (Table 3, Fig. 2 and Fig. S1). It is very closer than expected for charge assisted C—H···Cg (edge to face) intermolecular interactions (Table 3 and Fig. S1) [24]. The compound was further formed a 3-D network through intermolecular interactions (Fig. S1).

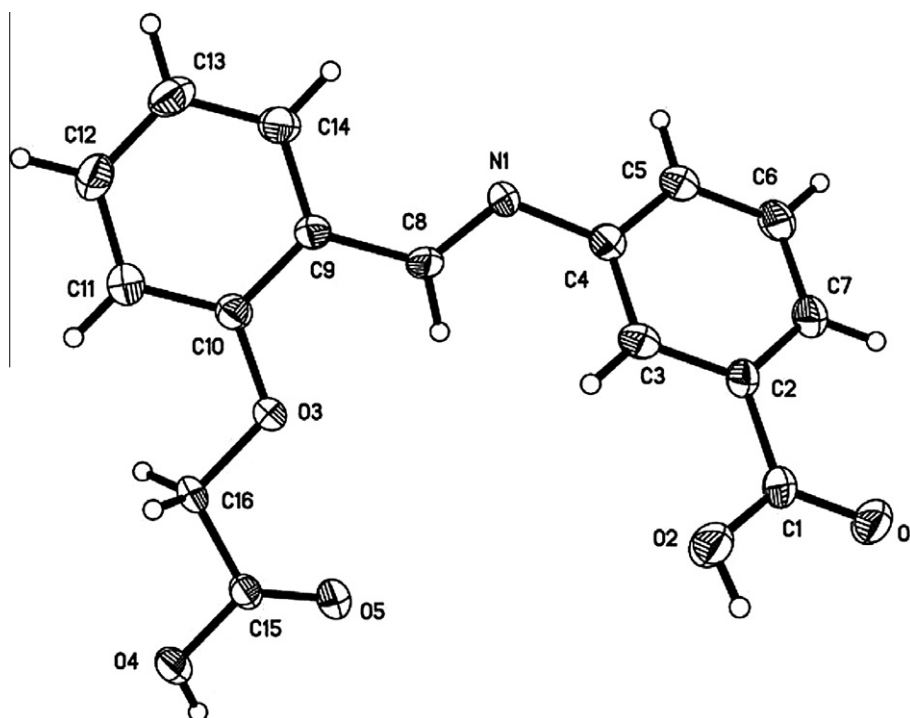


Fig. 1. The molecular structure of the title compound 1.

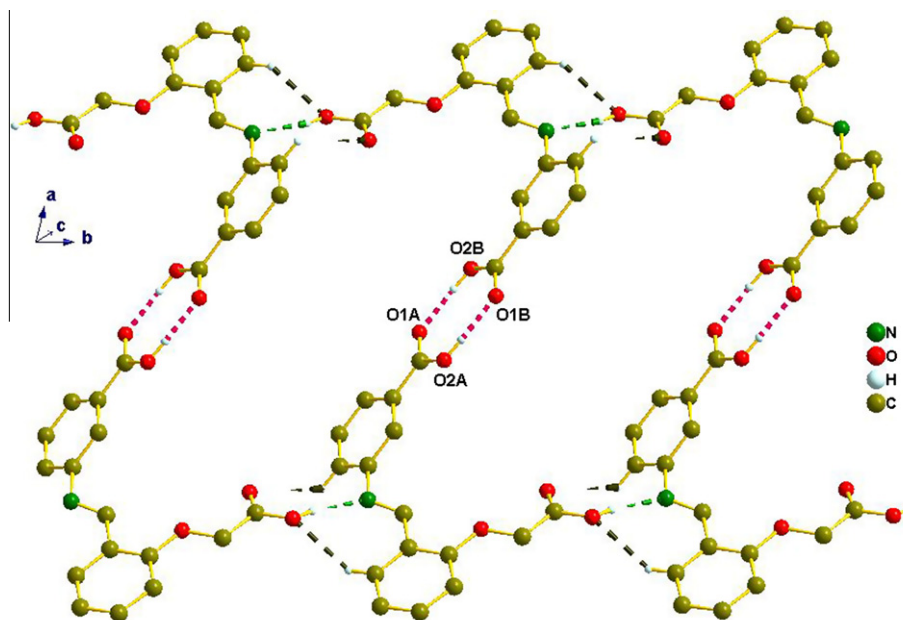


Fig. 2. Part of the crystal structure of the title molecule, showing the formation of centrosymmetric $R_2^2(8)$ dimer. Part atoms were omitted, the hydrogen bonds are indicated by dotted lines.

Table 3
Hydrogen bonding of **1** (Å, °).

D—H...A	d(D—H)	d(H...A)	<DHA	d(D...A)	Symmetry codes
O2—H2...O1 ⁽ⁱ⁾	0.86	1.77	174	2.63	(i): 2 - x, 1 - y, 2 - z
O4—H4...N1 ⁽ⁱⁱ⁾	0.86	1.92	160	2.75	(ii): x, y + 1, z
C3—H3...O4 ⁽ⁱⁱⁱ⁾	0.93	2.62	144	3.41	(iii): 1 - x, 2 - y, 1 - z
C5—H5...O5 ^(iv)	0.93	2.89	118	3.42	(iv): x, -1 + y, z
C7—H7...O5 ^(v)	0.93	2.55	125	3.18	(v): 1 - x, 1 - y, 2 - z
C14—H14...O4 ^(iv)	0.93	2.42	141	3.19	
C16—H16B...O5 ⁽ⁱⁱⁱ⁾	0.97	2.80	122	3.41	
D—H...A	d(D—H)	d(H...Cg)	<DHCg	d(D...Cg)	Symmetry codes
C16—H16A...Cg ^(vi)	0.97	2.92	128	3.59	Cg: C9/ C10/C11/ C12/C13/ C14 ring, (vi): -x, 2 - y, 1 - z

3.2. UV-vis spectrum

The UV-vis spectra of the compound were measured in *N,N*-dimethyl formamide solution with concentration of 1.0×10^{-4} M ($1 \text{ M} = 1 \text{ mol L}^{-1}$). The computation of UV-vis was processed using the density functional theory (DFT) method at the B3LYP and 6-31+G(d) basis set in Gaussian 03 W software package. The sharp and strong high-energy absorption bands at 321 nm are assigned as $n-\pi^*$ transition from HOMO-1 \rightarrow LUMO of the C=N group [26].

Table 4
Comparison of experimental and theoretically predicted IR frequencies.

Assignment	Experimental frequency	Calculated frequency	
		RB3LYP/6-31+G(d)	RHF/6-31G*
O—H str.	3431	3206	3267
C—H asym-str.	3079	3066	3087
C—H sym. str.	2918	3026	3036
C=O str. + O—H rock.	1760	1789	1789
C=O str.	1678	1689	1672
C=N str.	1605	1629	1624
C—C str.	1582	1627	1587
C=C str.	1542	1534	1548
C—H bend.	1487	1494	1521
C—H rock.	1431	1423	1441
O—H rock. + C—C str.	1380	1376	1375
O—H rock.	1225	1221	1227
C—O str.	1070	1094	1091
Ring (phenyl) breath	919	926	924
OCO bend	757	776	764

3.3. Fluorescence spectrum

Photoluminescent measurements of the title compound were carried out in *N,N*-dimethyl formamide solution with concentration of 5.0×10^{-5} M at room temperature. The compound DFT calculations were started from optimized geometry using the B3LYP/6-31+G(d) level of theory and were performed for gas phase to calculate excitation energies. The photoluminescent spectrum of the title compound is depicted in Fig. 3. It can be seen that the intense purple fluorescence emission at 409 nm from HOMO to LUMO ($\lambda_{\text{ex}} = 344$ nm) and a moderate intensity luminescence with emission maximum at 409 nm ($\lambda_{\text{ex}} = 275$ nm) and may be attributable to $\pi-\pi^*$ transitions [27]. The value of excitation energy at 344 nm rise from HOMO-1 to LUMO transitions. The emission in

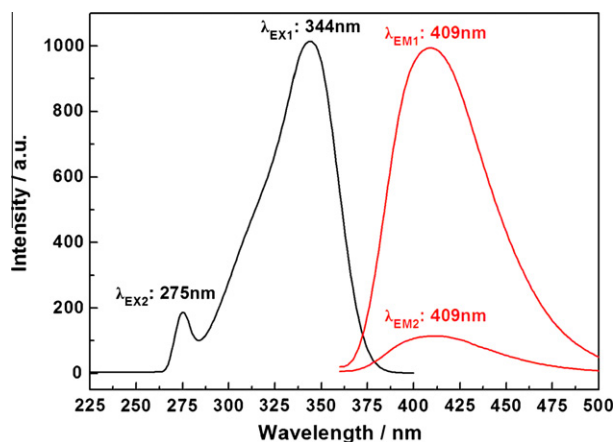


Fig. 3. The fluorescence of compound.

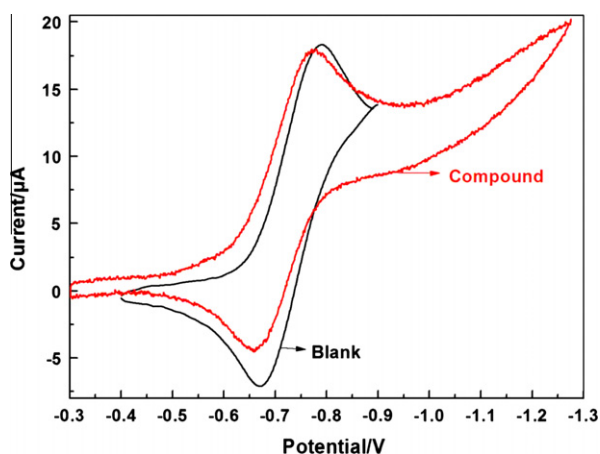


Fig. 4. Cyclic voltammogram of 1.0×10^{-4} M compound 1.

the ultraviolet region indicates that compound appears to be good candidate for promising purple-light emitting material.

3.4. Electrochemistry

Fig. 4 depicts the cyclic voltammogram of the title compound in *N,N*-dimethyl formamide solution containing of 0.1 M tetrabutylammonium bromide at scan rate 0.03 V s^{-1} . The oxidation-reduction peaks vest in the conductive medium redox reaction. The anodic peak and cathodic peak of the title compound are not mutativer more feckly than the blank, indicates that the electrochemical behavior of the title compound on the glass carbon electrode is very stable, and which oxidation–reduction reaction is difficult. This is consistent with the frontier molecular orbitals analysis results.

3.5. Geometry optimization

The optimized parameters of the title compound (bond lengths and angles, and dihedral angles) by RB3LYP/6-31+G(d) and RHF/6-31G* methods are listed in Table 2 and compared with the experimental crystal structure for the title compound.

Most of the optimized bond lengths, bond angles and torsion angles are slightly longer than the experimental values, because the theoretical calculations are based on the isolated molecules in the gaseous phase, while the experimental results are based

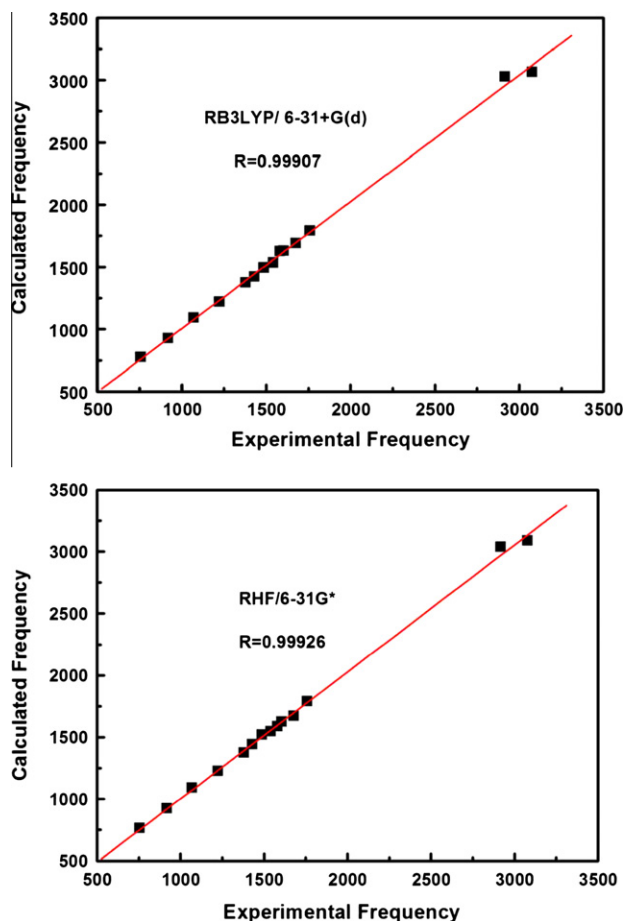


Fig. 5. Correlation graphics of calculated and experimental frequencies of the title compound.

on the molecules in the solid state. In solid state, the existence of the crystal field along with the intermolecular interactions have connected the molecules together, which result in the differences of bond parameters between the calculated and experimental values [28]. However, in general, the predicted bond lengths, angles and torsion angles are still in agreement with the values based upon the X-ray crystal structure data, which indicates that calculated geometric parameters were reasonable highly and they are the bases for calculating other parameters, such as Mulliken charge analysis, Wiberg bond index analysis and frontier molecular orbitals (FMOs), molecular electrostatic potential (MEP), as we described below.

3.6. Vibrational frequency

Some primary experimental IR data and calculated frequencies are listed in Table 4. The descriptions concerning the assignment [24] have also been indicated in the Table 4. To make comparison with experiment, we present correlation graphics in Fig. 5 based on the calculations. As we can see from correlation graphic in Fig. 5, experimental fundamentals are agreement with the scaled fundamentals. As a result, the predicted harmonic vibration frequencies and the experimental data are very similar to each other. In a word, the scaled frequencies of the DFT and HF calculations are close to the corresponding FT-IR vibration data and on the whole the RB3LYP/6-31+G(d) and RHF/6-31G* levels can predict the vibrational frequencies for the system studied here.

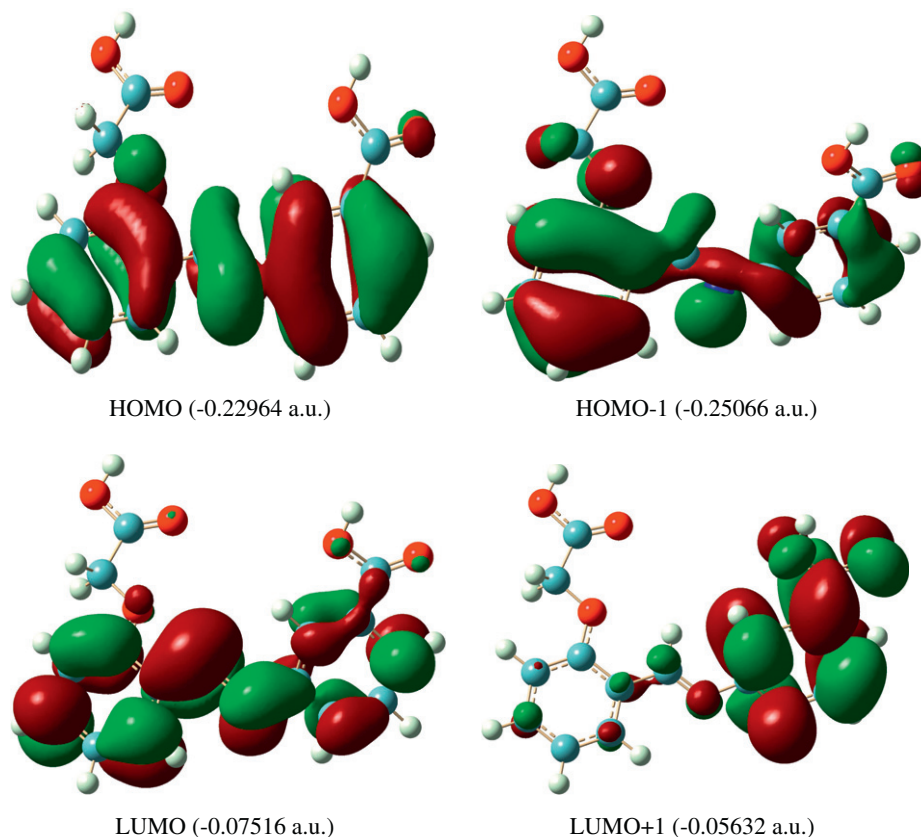


Fig. 6. Molecular orbital surfaces and energy levels of 1.

3.7. Frontier molecular orbitals

The frontier molecular orbitals play an important role in the electric and optical properties, as well as in UV–vis spectra, fluorescence spectrum and chemical reactions [29]. Fig. 6 shows the distributions and energy levels of the HOMO–1, HOMO, LUMO and LUMO+1 orbitals computed at the RB3LYP/6-31+G(d) level for

the title compound. E_{HOMO} is often associated with the electron donating ability of the molecule. High values of E_{HOMO} are likely to indicate a tendency of the molecule to donate electrons to appropriate acceptor molecules with low-energy, empty molecular orbital. Therefore, the energy of the lowest unoccupied molecular orbital (E_{LUMO}) indicates the ability of accepting electrons to molecule [30]. The eigenvalues of LUMO and HOMO and their energy

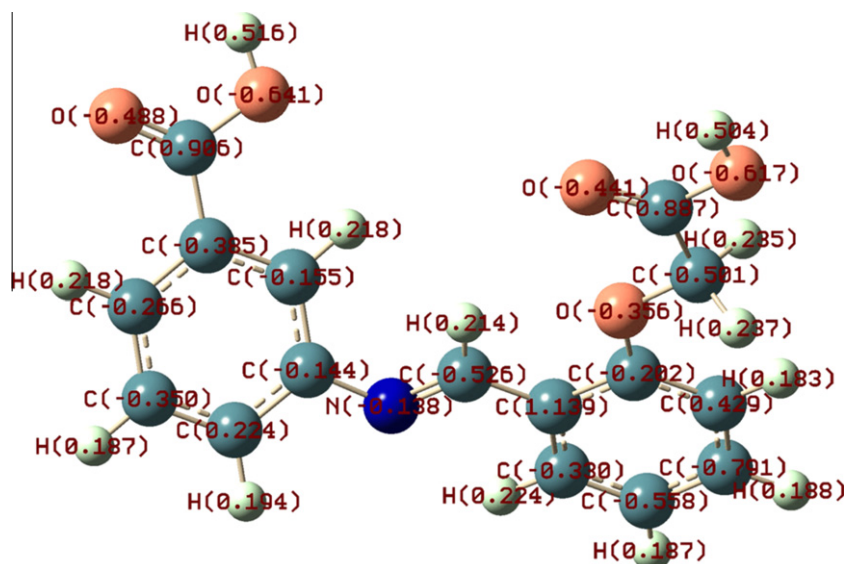


Fig. 7. The Mulliken charge population of 1.

Table 5
Selected calculate wiberg of the title compound.

Wiberg	Bond indexes	
	RB3LYP/6-31+G(d)	RHF/6-31G*
W _{C8N1}	1.7629	1.8127
W _{C4N1}	1.0992	1.0434
W _{C8C9}	1.0908	1.0462
W _{C1C2}	1.0197	1.0005
W _{C2C3}	1.3859	1.3858
W _{C3C4}	1.3688	1.3956
W _{C4C5}	1.3528	1.3724
W _{C5C8}	1.4475	1.4480
W _{C7C8}	1.4361	1.4302
W _{C2C7}	1.3698	1.3902
W _{C1O1}	1.7214	1.6886
W _{C1O2}	1.0354	0.9954
W _{C10O3}	0.9982	0.9576
W _{C16O3}	0.9137	0.8963

3.8. Mulliken charge analysis

Mulliken charge is related to the electronic density and is a very useful descriptor in understanding sites for electrophilic attack and nucleophilic reactions as well as hydrogen bonding interactions [34–36]. Electric charges in the molecule are obviously responsible for electrostatic interactions. The local electron densities or charges are important in many chemical reactions and for physico-chemical properties of compounds [37]. In order to predict reactive sites for electrophilic attack for the title compound, Mulliken charge was calculated at the RB3LYP/6-31G+(d) level and shown in Fig. 7. As easily can be seen in Fig. 7, the O atoms and N atoms take on major negative net charges, so the net charges of the carboxyl O atoms are more negative than that of the N atoms, showing the carboxyl are mainly active region. When compounds fall across metal, carboxyl will first provide electronic to metal atoms form the stable chemical bonds.

3.9. Wiberg bond index analysis

Wiberg bond index analysis has been used to evaluate the type of bands in title compound. Selected wiberg bond index for compound are listed in Table 5. The values of bond order of C4–N1, C10–O3, C16–O3 and C8–C9 are obviously close 1.0000, respectively, showing these bonds are one-touch. In phenyl ring, the C–C bonds are typical the conjugate structure. However, the band C1–O1 and C8–N1 are double-bonds attributed to the bond order of C1–O1 and C8–N1 are larger than 1.5000, which is consistent with the conclusion that the shorter the bond length, the larger the bond order leading to the stronger the bond. Simultaneously, this result is consistent with the results of the crystallographic data of compound.

3.10. Molecular electrostatic potential

Molecular electrostatic potential (MEP) is related to the electronic density and is a very useful descriptor in understanding sites for electrophilic attack and nucleophilic reactions as well as hydrogen bonding interactions [24]. To predict reactive sites for electrophilic attack for the title compound, MEP was calculated at the RB3LYP/6-31+G(d) optimized geometry. The negative (red)¹ regions of MEP were related to electrophilic reactivity and the positive (blue) ones to nucleophilic reactivity shown in Fig. 8. As easily can be seen in Fig. 8, this molecule has four possible sites for electrophilic attack. The negative regions are mainly over the O1, O2, O5 and N1 atoms. For the title compound, negative regions were calculated: the MEP value around O1 is more negative than that of O2, O5 and N1 atoms. When compounds molecular meet metal atoms, carboxyl oxygen atoms (O1) provide electric charges more easily to the metal atoms unfilled and full electronic track the formation of coordination bonds key. This is consistent with the frontier molecular orbitals analysis results.

4. Conclusion

In this study, a detailed analysis of the title compound was performed according to its crystal structure, theoretical and experimental FT-IR, fluorescence, and UV-vis absorption. Crystallographic analysis reveals that the non-covalent C–H...Cg intermolecular interactions and intermolecular hydrogen bonding interactions form 3D net in the title compound. The geometric parameters of the title compound obtained using the RB3LYP/

¹ For interpretation of color in Fig. 8, the reader is referred to the web version of this article.

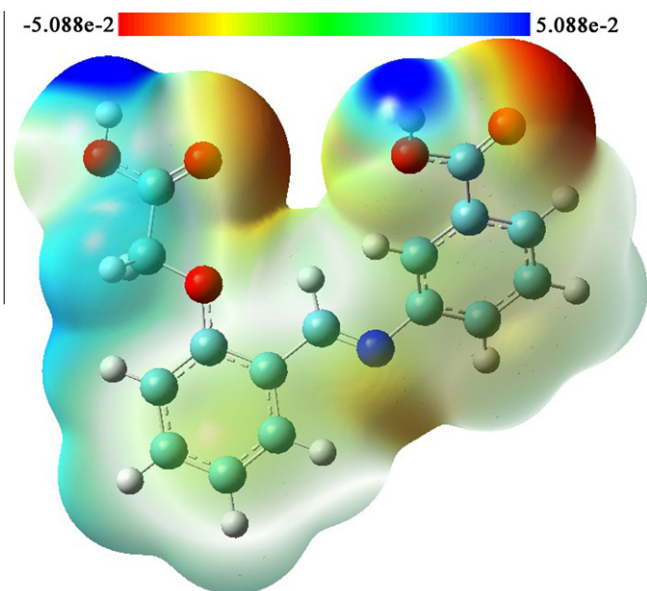


Fig. 8. Molecular electrostatic potential map calculated at RB3LYP/6-31G+(d) level.

gap reflect the coordination ability with the metal of the molecule. The calculated self-consistent field (SCF) energy of compound is -1048.45344801 a.u. and the value of the energy separation between the HOMO and LUMO is 0.15448 a.u. Contrast to literature [31–33], compound molecules with smaller ΔE and higher E_{HOMO} , showed that compounds with metal happen more easily into key reaction. In addition, the eigenvalues of LUMO and HOMO and their energy gap reflect the biological activity of the molecule. The decrease in the HOMO and LUMO energy gap explains the eventual charge transfer interaction taking place within the molecule which is responsible for the bioactivity of the molecule.

As can be seen from Fig. 6, the HOMO corresponds to the π -orbital of the intra-annular double bond; while LUMO+1 corresponds to the π -antibonding type orbital. It is apparent that for both of these there is some degree of π - π overlap. The HOMO is located on the two benzene rings and C=N group. The LUMO is located on the benzene rings of *o*-formylphenoxyacetic acid and C=N group. The value of the energy separation between the HOMO and LUMO is 0.15448 a.u. and this energy gap indicates that the oxidation-reduction of title compound is stable, which was conformed with results of electrochemistry analysis.

6-31+G(d) and HF/6-31G* methods match well with the X-ray diffraction data. Considering DFT calculations, it can be said that the experimentally observed excitation energy at 344 nm correspond to HOMO–1 → LUMO transitions, and fluorescence emission at 409 nm from HOMO to LUMO transitions. Experimental electronic absorption bands at 321 nm are assigned as $n-\pi^*$ transition from HOMO–1 → LUMO of the C=N group. Correspondingly, the wiberg bond index was performed, the calculation results are good agreed with experimental data. Molecular electrostatic potential (MEP), where the negative potential located on O1, O2, O5 and N1 atoms highlights its behavior as a strong proton acceptor regions. The lowering of the HOMO–LUMO energy gap value has substantial influence on the intramolecular charge transfer, coordination ability and bioactivity of the molecule. Furthermore, the electrochemical studies reveal that redox reaction of the title compound is very difficult in N, N-dimethyl formamide solution.

Acknowledgements

This work was supported by the Key Laboratory of Environmental Engineering, Protection and Assessment of Guangxi, the National Water Pollution Control and Management of China (No. 2008ZX07317-02) and Guangxi Natural Science Foundation (No. 2012GXNSFAA053034).

Appendix A. Supplementary material

Supplementary data associated with this article can be found, in the online version, at <http://dx.doi.org/10.1016/j.molstruc.2012.10.028>.

References

- [1] V. Alexander, Chem. Rev. 95 (1995) 273.
- [2] M.A. Affan, B.A. Fasihuddin, Y.Z. Liew, S.W. Foo, J. Ismail, J. Sci. Res. 1 (2009) 306.
- [3] R. Dinda, P. Sengupta, S. Ghash, T.C.W. Mak, Inorg. Chem. 41 (2002) 1684.
- [4] A. Sreekanth, U.L. Kala, C.R. Nayar, M.R.P. Kurup, Polyhedron 23 (2004) 41.
- [5] N. Tezer, N. Karakus, J. Mol. Model. 15 (2009) 223.
- [6] P.B. Sreeja, M.R.P. Kurup, A. Kishore, C. Jasmin, Polyhedron 23 (2004) 575.
- [7] W.P. Jia, J.G. Yang, F. Li, F.Y. Pan, J. Inorg. Chem. 24 (2008) 627.
- [8] J.G. Yang, F.Y. Pan, W.P. Jia, F. Li, J. Inorg. Chem. 25 (2009) 2207.
- [9] X.Q. Shen, Z.J. Li, H.Y. Zhang, Y.F. Zhou, K. Liu, Q.A. Wu, E. Wang, Thermochim. Acta 428 (2005) 77.
- [10] Ç. Albayrak, B. Koşar, S. Demir, M. Odabasoglu, O. Buyukgungor, J. Mol. Struct. 963 (2010) 211.
- [11] Ç. Albayrak, R. Frank, J. Mol. Struct. 984 (2010) 214.
- [12] M.N. Xanthopoulou, S.K. Hadjikakou, N. Hadjiladis, Eur. J. Med. Chem. 43 (2008) 327.
- [13] W. Rehman, A. Badshah, M.K. Baloch, Eur. J. Med. Chem. 43 (2008) 2380.
- [14] F.D. Proft, P. Geerlings, Chem. Rev. 101 (2001) 1451.
- [15] D.W. Emmons, Organic Synthesis, John Wiley and Sons Inc., New York, 1966, vol. 46.
- [16] G.M. Sheldrick, Acta Cryst. A 46 (1990) 467.
- [17] G.M. Sheldrick, SHELXL-97™ Program for Crystal Structure Refinement, University of Göttingen, Germany, 1997.
- [18] A.D. Becke, J. Chem. Phys. 98 (1993) 5648.
- [19] M.J. Frisch, G.W. Trucks, H.B. Schlegel, G.E. Scuseria, M.A. Robb, J.R. Cheeseman, J.A. Montgomery, Jr., T. Vreven, K.N. Kudin, J.C. Burant, J.M. Millam, S.S. Iyengar, J. Tomasi, V. Barone, B. Mennucci, M. Cossi, G. Scalmani, N. Rega, G.A. Petersson, H. Nakatsuji, M. Hada, M. Ehara, K. Toyota, R. Fukuda, J. Hasegawa, M. Ishida, T. Nakajima, Y. Honda, O. Kitao, H. Nakai, M. Klene, X. Li, J.E. Knox, H.P. Hratchian, J.B. Cross, V. Bakken, C. Adamo, J. Jaramillo, R. Gomperts, R.E. Stratmann, O. Yazyev, A.J. Austin, R. Cammi, C. Pomelli, J.W. Ochterski, P.Y. Ayala, K. Morokuma, G.A. Voth, P. Salvador, J.J. Dannenberg, V.G. Zakrzewski, S. Dapprich, A.D. Daniels, M.C. Strain, O. Farkas, D.K. Malick, A.D. Rabuck, K. Raghavachari, J.B. Foresman, J.V. Ortiz, Q. Cui, A.G. Baboul, S. Clifford, J. Cioslowski, B.B. Stefanov, G. Liu, A. Liashenko, P. Piskorz, I. Komaromi, R.L. Martin, D.J. Fox, T. Keith, M.A. Al-Laham, C.Y. Peng, A. Nanayakkara, M. Challacombe, P.M.W. Gill, B. Johnson, W. Chen, M. W. Wong, C. Gonzalez, J.A. Pople, Gaussian 03, Revision E.01, Gaussian, Inc., Wallingford CT, 2004.
- [20] J.S. Murray, T. Brinck, M.E. Grice, P. Politzer, J. Mol. Struct.: Theochim 256 (1992) 29.
- [21] F.H. Allen, O. Kennard, D.G. Watson, L. Brammer, A.G. Orpen, R. Taylor, J. Chem. Soc. Perkin Trans. 2 (1987) S1.
- [22] J. Casanovas, A.M. Namba, S. León, G.L.B. Aquino, J. Org. Chem. 66 (2001) 3775.
- [23] J.P. Jasinski, R.J. Butcher, M.T. Swamy, B. Narayana, B.K. Sarojini, H.S. Yathirajan, J. Chem. Crystallogr. 40 (2010) 25.
- [24] S. Demir, M. Dincer, E. Korkusuz, İ. Yıldırım, J. Mol. Struct. 980 (2010) 1.
- [25] A. Ghosh, A. Sarkar, P. Mitra, et al., J. Mol. Struct. 980 (2010) 7.
- [26] R. Gup, B. Kirkan, Spectrochim. Acta Part A Mol. Biomol. Spectrosc. 64 (2006) 809.
- [27] S. Naskar, S. Naskar, R.J. Butcher, S.K. Chattopadhyay, Inorg. Chim. Acta 363 (2010) 404.
- [28] H. Tanak, Y. Köysal, Y. Ünver, M. Yavuz, Ş. Işık, K. Sancak, Struct. Chem. 20 (2009) 409.
- [29] I. Fleming, Frontier Orbitals and Organic Chemical Reactions, Wiley, London, 1976.
- [30] F. Kandemirli, S. Sagdinc, Corros. Sci. 49 (2007) 2118.
- [31] J. Fang, J. Li, J. Mol. Struct.: Theochim 593 (2002) 179.
- [32] H. Luo, Y.C. Guan, K.N. Han, Corrosion 54 (1998) 721.
- [33] M. Behpour, S.M. Ghoreishi, N. Mohammadi, N. Soltani, M. Salavati-Niasari, Corros. Sci. 52 (2010) 4046.
- [34] N.A. Ogorodnikova, J. Mol. Struct.: Theochim 894 (2009) 41.
- [35] F.J. Luque, J.M. López, M. Orozco, Theor. Chem. Acc. 103 (2000) 343.
- [36] N. Okulik, A.H. Jubert, Internet Electron. J. Mol. Des. 4 (2005) 17.
- [37] G. Gece, Corros. Sci. 50 (2008) 2981.